MagicPlate-512: a two dimensional silicon detector array for Quality Assurance of stereotactic motion adaptive radiotherapy

M. Petasecca[1,6], M.K. Newall[1,6], J.T. Booth[2,3], M. Duncan[1], A.H. Aldosari[1,6], I. Fuduli[1,6], A.A. Espinoza[1,6], C.S. Porumb[1,6], S. Guatelli[1,6], P. Metcalfe[1,6], E. Colvill[2,3], D. Cammarano[1], M. Carolan[1,4,6], B. Oborn[1,4], M.L.F. Lerch[1,6], V. Perevertaylo[1], P.J. Keall[2], A.B. Rosenfeld[1,6]

[1]Centre for Medical Radiation Physics – University of Wollongong, NSW 2500, Australia

[2]School of Medicine, University of Sydney, NSW 2006, Australia

[3]Northern Sydney Cancer Centre, Royal North Shore Hospital, NSW 2065, Australia

[4]Illawarra Cancer Care Centre, Wollongong Hospital, NSW 2500, Australia

[5]SPA-BIT, Kiev 02232, Ukraine

[6]Illawarra Health Medical Research Institute, Wollongong, NSW 2522, Australia

Abstract

Purpose: Spatial and temporal resolutions are two of the most important features for quality assurance instrumentation of motion adaptive radiotherapy modalities. The goal of this work is to characterise the performance of the two-dimensional high spatial resolution monolithic silicon diode array named "MagicPlate-512" for Quality Assurance of Stereotactic Body Radiation Therapy (SBRT) and Stereotactic Radiosurgery (SRS) combined with a dynamic multi leaf collimator (MLC) tracking technique for motion compensation.

Methods: MagicPlate-512 is used in combination with the movable platform HexaMotion and a research version of radiofrequency tracking system Calypso driving MLC tracking software. We reconstruct 2D dose distributions of small field square beams in three modalities: in static conditions, mimicking the temporal movement pattern of a lung tumor, and tracking the moving target while the MLC compensates almost instantaneously for the tumor displacement. Use of Calypso in combination with MagicPlate-512 requires a proper radiofrequency interference shielding. Impact of the shielding on dosimetry has been simulated by Geant 4 and verified experimentally. Temporal and spatial resolution of the dosimetry system allows also for accurate verification of segments of complex stereotactic radiotherapy plans with identification of the instant and location where a certain dose is delivered. This feature allows for retrospective temporal reconstruction of the delivery process and easy identification of error in the tracking or the multileaf collimator driving systems. A sliding MLC wedge combined with the lung motion pattern has been measured. The ability of the MP512 in 2D dose mapping in all three modes of operation was benchmarked by EBT3 film.

Results: Full width at half maximum and penumbra of the moving and stationary dose profiles measured by EBT3 film and MagicPlate-512 confirm that motion has a significant impact on the dose distribution. Motion, no motion and motion with MLC tracking profiles agreed within 1 mm and 0.4 mm, respectively, for all field sizes tested. Use of electromagnetic tracking system generates a fluctuation of the detector baseline up to 10% of the full scale signal requiring a proper shielding strategy. MagicPlate-512 is also able to reconstruct the dose variation pulse-by-pulse in each pixel of the detector. An analysis of the dose transients with motion and motion with tracking shows that the tracking feedback algorithm used for this experiment can compensate effectively only the effect of the slower transient components. The fast changing components of the organ motion can contribute only to discrepancy of the order of 15% in penumbral region while the slower components can change the dose profile up to 75% of the expected dose.

Conclusions:

MagicPlate-512 is shown to be, potentially, a valid alternative to film or 2D ionizing chambers for Quality Assurance dosimetry in SRS or SBRT. Its high spatial and temporal resolution allows for accurate reconstruction of the profile in any conditions with motion and with tracking of the motion. It shows excellent performance to reconstruct the dose deposition in real time or retrospectively as a function of time for detailed analysis of the effect of motion in a specific pixel or area of interest.

I. Introduction

Radiotherapy is one of the main methods used besides chemotherapy and surgery for cancer treatment. Modern radiotherapy aims to deliver sufficient dose of ionising radiation to tumors in order to achieve the desired therapeutic outcome, while at the same time minimising potential damage to surrounding healthy tissue. Conformal radiotherapy shapes the treatment beam to match the shape of the tumor projection from any beam direction. Stereotactic Radio Surgery (SRS) and Stereotactic Body Radiation Therapy (SBRT) extend this concept by uniting high precision image guidance at treatment with higher 'ablative' dose per fraction and fewer fractions than conventional radiotherapy. SBRT has been implemented widely for lung, spine, liver and prostate cancer treatment [1]. The advantages of these techniques can, however, be compromised by tumor movement both in between (inter-fraction) and during (intra-fraction) treatment fractions. Lung tumors have been reported to move up to 25-30 mm [2] which implies that treatment volume margins need to be enlarged to encompass the full movement, at the cost of increasing dose to healthy tissue. Strategies for ensuring dosimetric coverage by minimising the Planning Target Volume (PTV) margin, can now be individualized to a specific patient's geometry with customized margins using Imaged Guided Radiation Therapy (IGRT). Other strategies incorporate continuous monitoring of tumor movements to gate or modify the beam, known as Adaptive RT (ART). Respiratory gating, one application of this strategy, has the disadvantage of longer treatment times since the beam is fired only when the tumor is within a predefined range [3]. Additionally with gating strategies, the intermittent rotating of a heavy gantry quickly and repeatedly can put undue mechanical stress on the equipment affecting its reliability.

Several solutions have been proposed to reduce the effect of target motion, without increasing significantly treatment time or linac maintenance costs. Technologically advanced approaches to target motion compensation come from solutions such as CyberKnife (Accuray Inc. – CA, USA) and Vero SBRT (Brainlab GA – Feldkirchen, Germany) which adopt a robotic arm [3] and a gimbaled irradiation head, respectively, to adjust the photon beam source position in real time and match the moving target volume. Because they both require an imaging guidance equipment for identification of the target position, already embedded in the machines, they are expensive and this makes their availability limited.

Real time adaptation is possible on the standard linac through couch tracking and MLC tracking of a real time position signal [4]. Falk et al. [5] utilises the optical real-time organ tracking of Real-time Position Monitoring (RPM, Varian Medical Systems) to detect reflective markers applied to the patient's skin. This technique has been combined with the RapidArc IMRT system and MLC tracking. The limitation of such an approach is mainly related to the potential for differences between the displacement of the exterior surface of the body and the internal tumor motion path in 3D, especially

85   intra-fraction. Simulation of such scenario by a rigid body such as a water equivalent phantom fails to help evaluate the effect of such relative displacement.

An alternative attractive solution which takes into account the actual tumor movement is proposed by Keall et al [2]. Continuous monitoring of the organ motion is possible using the Calypso 4D Localisation System (Varian Medical Systems – Palo Alto, USA), which uses implanted

90   radiofrequency (RF) transponder circuits referred to as beacons. An RF signal is emitted by Calypso at a frequency of approximately 300-500 kHz and excites the beacons which act as dipoles [2],[6]. The electromagnetic signal generated by the dipoles is detected by an array of coils positioned above the patient and the relative distance of each beacon from the array is recorded. Using a minimum of three beacons, it is possible to 3D reconstruct the position of the centre of mass of the three transponders

95   implanted into the organ. The position data is sent to the tracking system which drives the DMLC. The position of the Calypso array with respect to the linac is determined by Infra Red (IR) cameras within the treatment room [2], and gives the instantaneous relative position of the organ in respect to the DMLC. Feedback algorithm for calculation of the DMLC tracking kinematics based on the data provided by Calypso has been developed by Keall et al. [2]. This technique has been implemented

100   successfully in clinical practice [7].

Smith et al. [8] have investigated the effectiveness of implantable RF transponders for DMLC tracking of Intensity Modulated Arc radiotherapy (IMAT) plans, which included lung and prostate motion based on patient data. They found that the dose delivered with 4D DMLC tracking is equivalent to dose distribution delivered with gating treatment method but with a 2-4 fold increase in treatment

105   delivery efficiency when compared to gating. Sawant et al. [9] shows, with a similar tracking setup, that system geometric accuracy to be of the order of 2 mm for lung and 1 mm for prostate motion by using EPID. This approach has been used to evaluate the temporal and spatial resolution of the tracking system and its latency due to the delay between the movement and the effective reaction (or response) of the DMLC, but it does not provide information of the dose distribution accurately for

110   comparison with the TPS.

SRS and SBRT are complex radiotherapy techniques that use very high hypofractionaction regimes [10] and as such, require accurate Quality Assurance to minimise delivery mistakes which could be potentially harmful for the patient. SBRT also uses irregular 3D dose maps with field size as small as 5 cm square and SRS has circular fields few mm in diameter. These techniques require QA dosimetry

115   instrumentation with high spatial resolution and with small sensitive volumes and short pitch, to provide accurate 2D dose information. Current ionization chambers used in arrays often have their response compromised by the volume averaging effect, if their active volume is large in comparison to the field size. Chambers with a volume in the order of $1mm^3$ and less are not sensitive enough and so require longer irradiation time. Recently, liquid filled ionisation chambers with a sensitive volume

120 of 2.3x2.3x0.5 mm^3 and pitch of approximately 2.5 mm (Octavius 1000 SRS, PTW – Germany) have been introduced and appear to be as a valid solution for high spatial resolution ionising chamber arrays [11].

The spatial resolution of the array is determined not just by the density of pixels (pitch), but also by the dimensions of the sensitive element which average the dose across its volume. Water equivalence

125 guarantees that when the dosimeter is stacked and arrayed, there is no significant perturbation of the photon beam while performing QA measurements in a water tank or solid water phantom. Plastic dosimeters exhibit water equivalence over a wide energy range (0.2-25 MeV) and feature a highly sensitive detector material, enabling small sensitive volume construction, which are generally linear in dose and are dose rate and energy independent [12]. A clinical prototype of a water equivalent, small

130 sensitive volume (1.6 mm^3) plastic scintillator was developed by Lacroix et al. it was constructed from BCF-12 plastic scintillator (Saint-Gobain) coupled to BCF-98 optical fibre strands. The scintillator is 2 mm long and has a diameter of 1 mm, which is glued to a 1 mm diameter optic fibre 1.7 m in length. The fibres sit in 1 mm diameter grooves drilled into a 30x30x5 cm^3 solid water block. The grooves allow for a tight fit to ensure there is minimal air between the solid water and the fibre.

135 This prototype featured 29 strands (corresponding to 29 sensitive volumes) with 1 cm spacing, allowing for sampling across the whole 30 cm wide solid water block. The optic fibres carry the photons emitted from the scintillator to a CCD readout system placed at the opposite end of the treatment couch. Cerenkov radiation is an issue for fibre dosimeters but has been minimised with a spectral discrimination technique [13], which uses only the blue and green channels of the CCD colour

140 mosaic. Dosimetric performance of such devices is remarkably good with excellent agreement when compared to ionising chambers or film [14]. They, however, still suffer severe limitations in the number of channels (due to the routing of the fibres), degradation of the light yield due to radiation damage and acquisition time which requires several seconds (up to 25 seconds for a 1 mm diameter Fiber Optic Dosimeter [13]) for an accurate estimation of the dose distribution.

145 Centre for Medical Radiation Physics has designed and developed the Magic Plate-512 (MP512), a monolithic diode array to meet the system requirements for QA in SBRT and SRS dosimetry including characterization of effect of motion where MP512 plays simultaneously the role of the dosimetric medium and the movable target. MP512 has been already successfully tested for static small field dosimetry [15] and this work presents in phantom characterisation of the device as a

150 dosimeter for real-time ART and specifically to investigate the performance of Calypso-guided MLC tracking and benchmark the results by comparison with radiochromic film dosimetry under the same conditions.

II. Materials and Methods
a. *Magic Plate 512 detector array*

155   The MP512 is a monolithic dosimeter array of 52 x 52 mm^2 of total area with 512, 0.5 x 0.5 mm^2 ion implanted planar diodes with pixel pitch of 2 mm, fabricated on a bulk p-type thin silicon substrate. The diodes are operating in a passive mode where no bias voltage is applied across the n+p junction. The silicon detector array is wire bonded to a thin printed circuit board (PCB - 500 μm thick) or alternatively embedded into the PCB carrier by the "drop-in" technology, a proprietary

160   packaging technique developed by CMRP for radiation detector and is covered by a thin layer of protective epoxy or thin polyamide film to minimise accidental damage. The PCB provides the support for connection of the sensor to the readout electronics. The detector was pre-irradiated on a Co-60 gamma source to a total dose of 40 kGy to stabilise its response. Pre-irradiation is required only once with minimal effect of annealing at room temperature.

165   *b. Data acquisition system*

      The data acquisition (DAQ) system of MP512 is based on a commercially available analogue front end named AFE0064 (Texas Instruments), composed of 64 current integrators providing an analogue differential output proportional to the charge accumulated in a capacitor during a configurable time frame. Each set of two AFEs are interfaced to a quad analogue-to-digital-converter,

170   synchronised by a Field Programmable Gate Array (FPGA) which manages also the readout USB2 communication protocol with the host computer. The AFE configuration are set electronically through a serial protocol interface (SPI) on the lowest gain available to span the full scale up to 9.6 pC with a resolution of 16 bit and a non-linearity less than 0.1% [16]. Each current integrator is equipped with a double sampler for subtraction of the baseline, a feature that is particularly important when a high

175   signal-to-noise ratio is required, such as in medical instrumentation. The DAQ system uses eight AFE0064 chips, for a total of 512 channels, allowing the acquisition of the whole detector signals synchronously with the linac (pulse-by-pulse) or by the generation of an internal trigger with frequency up to 10 kHz [17].

      c. Detector packaging

180   For the application of the MP512 detector in combination with Calypso, a custom designed RF shielding, had to be adopted to avoid large fluctuations of the signal baseline generated by the time varying electromagnetic field inducing current in the detector wiring and in the analogue front end electronics. Fig.1 shows a diagram of the MP512 packaging structure composed of a sequence of layers of 2 mm thick aluminium, 5 mm thick solid water and 5mm PMMA slabs placed above the

185   detector. The aluminium slab also extends above the electronics acting as a shielding box for the preamplifier boards. Its thickness has been determined by aiming for no more than 5% of the original power of the RF field to be transmitted through the aluminium sheet, taking into account the "skin effect" produced by conducting materials.

Tab.1 Main electromagnetic parameters for the aluminum RF shield

Parameter	Description	Typ. value	Units
ε_0	permittivity in free space	$8.854 \cdot 10^{-12}$	F/m
μ_0	permeability in vacuum	$4\pi \cdot 10^{-7}$	H/m
μ_r	relative permeability	1	for aluminum [18]
ω	angular frequency	$2\pi \cdot f$	Hz
σ	conductivity	$1.54 \cdot 10^5$	$(\Omega cm)^{-1}$ for aluminum [18]

190

In the approximation of a plane electromagnetic wave generated by Calypso at a frequency f equal to 300 kHz [6], incident perpendicularly on the aluminum plane, the skin depth is approximately $\delta = \sqrt{\frac{2}{\mu_0 \mu_r \sigma \omega}} = 234$ μm. For an attenuation of 99.9%, we must have

$$\frac{\boldsymbol{\varphi_0} exp\left(\frac{-z}{2.34 \cdot 10^{-4}}\right)}{\boldsymbol{\varphi_0}} = 0.001 \ \rightarrow z \approx 2\ mm$$

where φ_0 represents the intensity of the incident electromagnetic wave and z represents the

195   thickness of the aluminium slab which acts as RF shield; the combination of aluminium-solid water and PMMA slabs forms an equivalent water depth of 1.5 cm which corresponds to d_{max} for a 6MV photon beam. Similar approach is used in a single diode packaging for entrance dosimetry using metal envelope (brass or tungsten) and plastic to reproduce thickness equivalent to d_{max} for required MV photon energy [19].

a)

b)
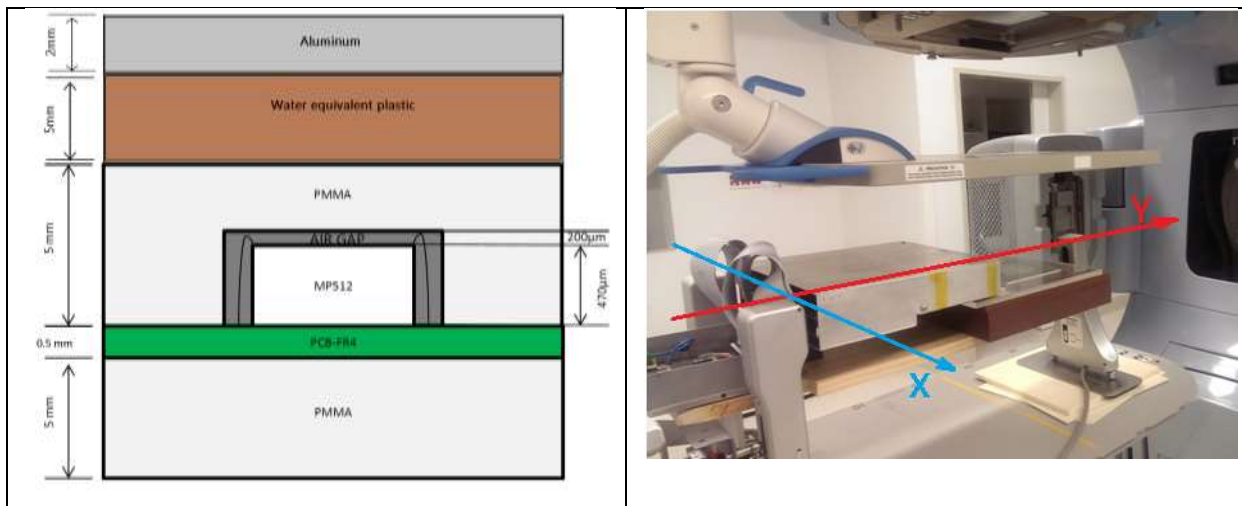
FIG. 1. a) Schematic of the MP512 packaging (not to scale); b) MP512, placed onto the platform HexaMotion underneath the coils' array of Calypso, is shown along with the orientation of the coordinate frame. The picture does not include the water equivalent plastic and the aluminium shield used during the tests to keep the silicon detector array position visible.

200

Monte Carlo Geant 4 version 10.0p01 [20] simulations were performed to determine the dose perturbation with the inclusion of 2 mm of aluminum on the surface of the detector enclosure for RF

shielding purposes. The beams 1x1 cm^2, 2x2 cm^2 and 3x3 cm^2 6 MV x-ray passing through a 30x30x30 cm^3 water block phantom were simulated. The reference simulation is when the entire phantom is water, while the simulation of interest includes replacing the first 2 mm water with aluminium, i.e. to replicate placing of 2 mm aluminium shielding above the PMMA detector enclosure. The source to surface distance (SSD) was 100 cm, and the beams were fired from phase space files created from an EGSnrc Monte Carlo based system that models a Varian 2100C linac. The model used to represent the linac and the phantom setup, along with the physics of transport, has been already validated by experimental results [21]. The physics processes modelled in the simulation are from the Geant4 electromagnetic Standard Physics Package and include photoelectric effect, Compton scattering and gamma conversion (photons), ionisation, Bremsstrahlung and positron annihilation (leptons). The particle range cut is set to 0.1 mm and the electron/positron maximum step length is 0.1 mm. Dose is scored inside the phantom at a voxel resolution of 1 mm^3. Each simulation is split into 10 parallel jobs each with unique seeds and the mean dose reported. The standard deviation is taken across 10 simulations to evaluate uncertainties. In total $4 \cdot 10^{13}$ primary histories are simulated for each field size, where the primary histories represents the number of electrons hitting the x-ray target in the linac head. The dose uncertainty is approximately ±1% of the dose at 1.5 cm depth at the beam central axis (CAX) for each field size.

The effectiveness of the aluminium shield has been measured by acquiring the baseline of the detector (dark signal) in three conditions: (a) with Calypso off, (b) with Calypso activated and MP512 unshielded and (c) with Calypso activated and the aluminium shielding placed at surface of the phantom as described above. Acquisition of the baseline has been performed for 120 seconds at sampling rate of 360 Hz, to allow for a large number of samples. Statistical analysis of the dark signal is performed calculating the average of the baseline and plotting the frequency distribution of its standard deviation in each channel of MP512 in the three different conditions.

d. Organ motion mimicking

Mimicking of the organ motion is performed by the means of the HexaMotion 6D moving platform (Fig.1b) manufactured by ScandiDos (Uppsala, Sweden) as accessory for Delta^4. A platform has been made by using a flat wood plate, with rigid connection to the HexaMotion, where MP512 and its DAQ have been placed above 6 cm of solid water for backscattering. HexaMotion allows the movement of the plate over five motion directions but, in this work, we have performed a study with a lung temporal movement pattern with components solely along the axis X and Y oriented as shown in Fig.1b. The pattern components are extracted from a real patient lung movement recorded by a 4D CT scan. The pattern is transferred to the motion platform by a text formatted file with absolute position frames (in the HexaMotion reference system) for X and Y every 25 ms. Fig.2 shows the overall

temporal pattern adopted for this study, which exhibits a baseline shift, and a zoom-out of the first 30 seconds is represented in the inset window.
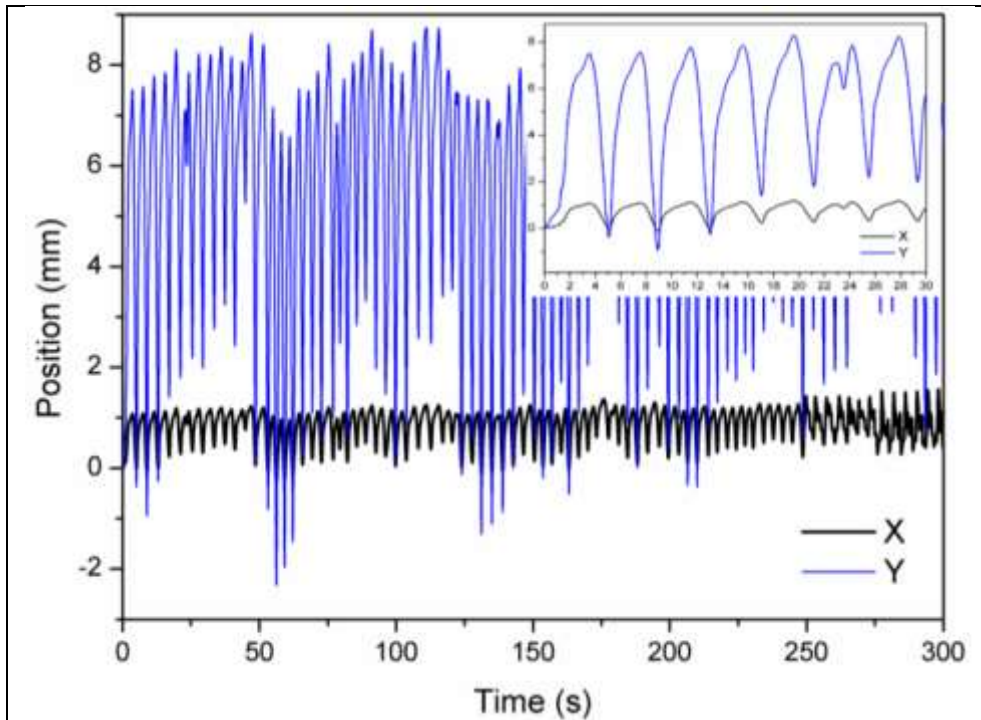

Fig.2: Lung temporal pattern X and Y components extracted from a patient 4D CT scan. The inset shows the details of the first 30 seconds of motion.

240   *e. Beam profile measurements*

Beam profiles of 1x1, 2x2 and 3x3 cm^2 are collimated by the MLC with the jaws retracted 1 cm in each direction to minimise the end-of-leaf leakages and to allow the full range of the movement which, in this work, is approximately 2 mm and 8 mm in X and Y directions, respectively. Dose profiles were measured along X and Y directions by MP512 and EBT3 films by irradiating them with

245   1000 MU, 6MV beam energy at 600 MU/min in three modalities: no motion, motion and motion with MLC tracking. Three RF beacons are attached to a thin plastic sheet at approximately a distance of 10 cm between them. The sheet is placed on top of the aluminium shield above the phantom during all measurements. The beacon triplet's centre of mass position is co-registered with the linac coordinate frame by Calypso.

250   In no-motion modality, the detector is aligned by the laser with the central pixels in coincidence with the isocentre with HexaMotion at its home position. The detector is placed on the movable platform above 6 cm of solid water and Calypso activated with no tracking functions and RF field activated.

In motion modality, the detector is aligned and in the same position as for the no-motion operation. Calypso is activated but with no tracking and the HexaMotion platform is running accordingly with

255   the lung temporal pattern described in section II.d, after being activated manually.

In motion with MLC tracking modality, the detector is on the phantom and moves along with the HexaMotion platform. Calypso tracks the position of the beacons and provides real-time position information to the University of Sydney MLC tracking software [7] which drives the MLC. No prediction was used.

260   All MP512 profiles were normalised to the response of the central pixel (row 11, column 12) and aligned with the corresponding EBT3 profile to the value at 50% of the central pixel response. The measurements for both detectors are calculated as the mean value of 5 repetitions of the same field delivery and the error bars of each data point are calculated as two standard deviations. The detector is equalised using the same technique adopted for MagicPlate-121 with a variation of the response

265   across the whole detector of 0.5% after equalisation [22].

Gafchromic EBT3 film (ASHLAND, Wayne, NJ) was used as the benchmark for the square beam profiles and the dynamic wedge integral dose measurements, in the three motion modalities. The EBT3 films were cut into sections of 10x10 cm^2 and positioned at the centre of the solid water phantom at d_{max} and isocentre. The film analysis method carried out for these measurements is the

270   same adopted in Aldosari et al. [15]. Particular care was taken to scan the film six times and use only the last three optical density maps [23], all scanned in the same orientation at the central region of the flatbed to reduce non-uniformities [24],[25].
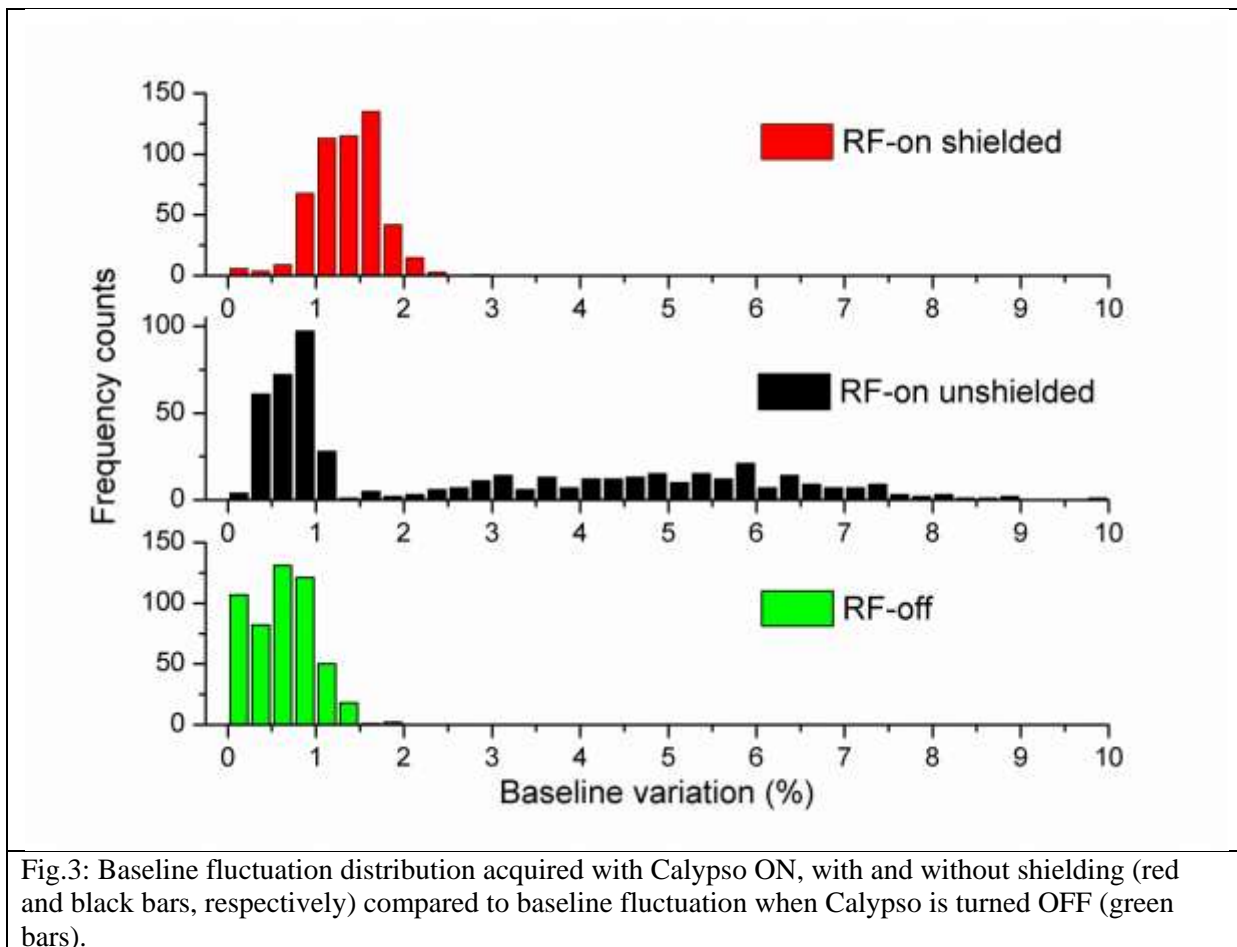
f. Evaluation of timing performance of MP512

The advantage of MP512 for dose Quality Assurance in motion adaptive radiotherapy is pulse-by-

275   pulse dosimetry. The high temporal resolution in dose mapping could be used to test and refine the performance of the feedback algorithm used to drive the DMLC to track the target motion measured by Calypso. 2D dose accumulation capability (X,Y and t) of MP512 has been investigated by delivering a dynamic wedge combined with the lung motion pattern described in Fig.2 to a solid water phantom placed onto the HexaMotion platform using the three motion modalities described above.

280   MP512 has been placed at 1.5 cm depth and central pixel aligned with the isocentre. The dynamic wedge has been formed by delivering in total 1000 MU at a dose rate of 600 MU/min and beam energy of 6 MV and by the means of the MLC motion with no rotation of the gantry. The predominant target motion component (Y direction) is along the direction of the MLC wedge and this allows ignoring the effects related to the lateral movements associated to the lung respiratory motion

285   (along X-direction). The gantry, fixed vertically above the detector, allows neglecting the effects of the angular response of the detector. The integral dose deposition measured by MP512 has been benchmarked with the dose response measured by EBT3 film exposed to the same beam and motion conditions. The instantaneous pulse-by-pulse and integral dose map measured by MP512 has been analysed in real time and retrospectively. The time response of the pixels corresponding to 50% of

290   maximum dose delivered with no motion was compared to time response of pixels with motion and
   motion with tracking with the same integral response.

III.   Results

   a.   Geant4 simulation of the detector enclosure and RF noise suppression performance

295   Diagrams in Fig.3 show that MP512, without shielding and in the presence of the RF
       interference generated by Calypso, measures baseline fluctuations up to 9% of the full signal scale
       when beam is delivered. This large fluctuation has a relative small frequency count with a maximum
       of 25 occurrences/second at 6% but it degrades the accuracy of the measurement substantially by the
       generation of a stochastic current signal summed to and undistinguishable from the signal generated
300   by the beam. Particularly, it affects the accuracy of the dose distribution in the penumbra and out of
       field. The red bars show the effect of the aluminium shielding which removes completely the large
       amplitude fluctuation component.

Fig.3: Baseline fluctuation distribution acquired with Calypso ON, with and without shielding (red
and black bars, respectively) compared to baseline fluctuation when Calypso is turned OFF (green
bars).

305   Figure 4 displays the results of the Monte Carlo study with Fig.4a showing the depth-dose profiles for
       each field size, while cross-profiles at 1.5 cm depth are presented in Fig.4b. The dosimetric impact of
       2 mm of aluminum shield placed on the detector enclosure is minimal; a very minor (within 1% of the
       simulation uncertainty) dose drop is seen in PDD measured by central pixel of MP512 in comparison
       with ionization chamber beyond 14 mm depth. No significant changes to the cross-profiles have been
310   observed for all fields. In the first 14 mm build up region there is a clear increase in the energy
       deposition in water as the aluminum (having density of approximately 2.7 g/cm^3) produces larger
       secondary electron fluence than the same thickness of water equivalent material.
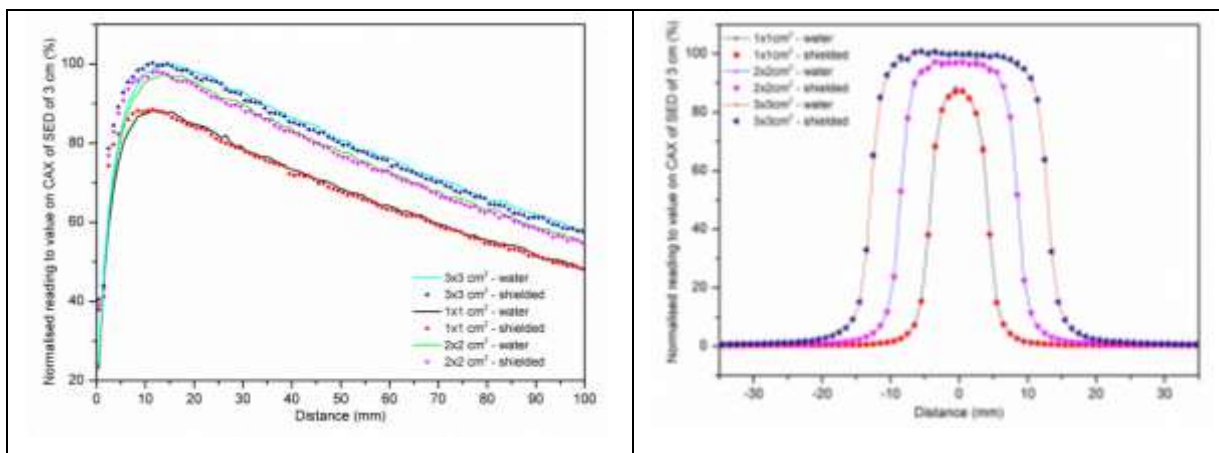
a)   b)

Fig.4: a) Comparison of the Geant4 simulations of Percentage Depth Dose (PDD) and b) dose
profiles for 1x1, 2x2 and 3x3 cm^2 field sizes with and without the aluminum shield. The response is
normalised to the central pixel response corresponding to the dose profile of 3x3 cm^2 radiation field.
Dot size represents the uncertainty of ±1%.

The results of the simulation study have been confirmed experimentally by measuring the PDD of a
315   6MV, 3x3 cm^2 beam by a Markus chamber (PTW – Germany) with and without the aluminum
       shielding and recording a discrepancy beyond the depth of 15 mm of approximately -1% (Fig.4c).
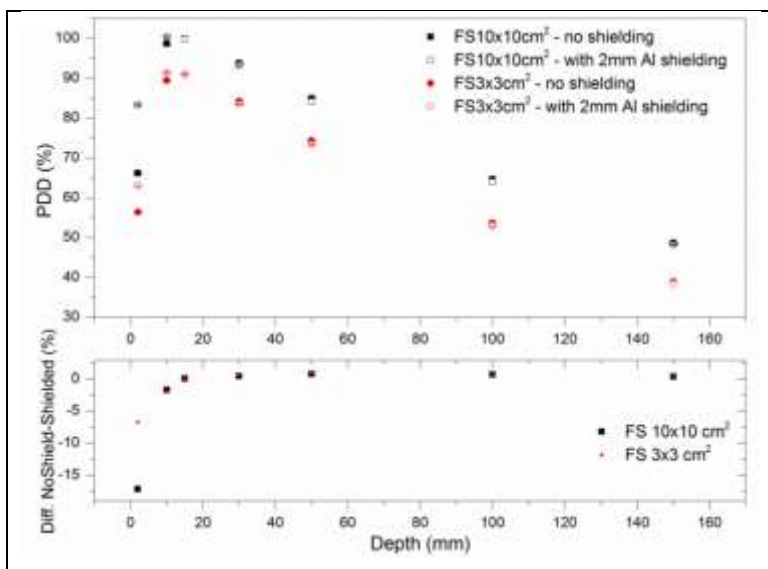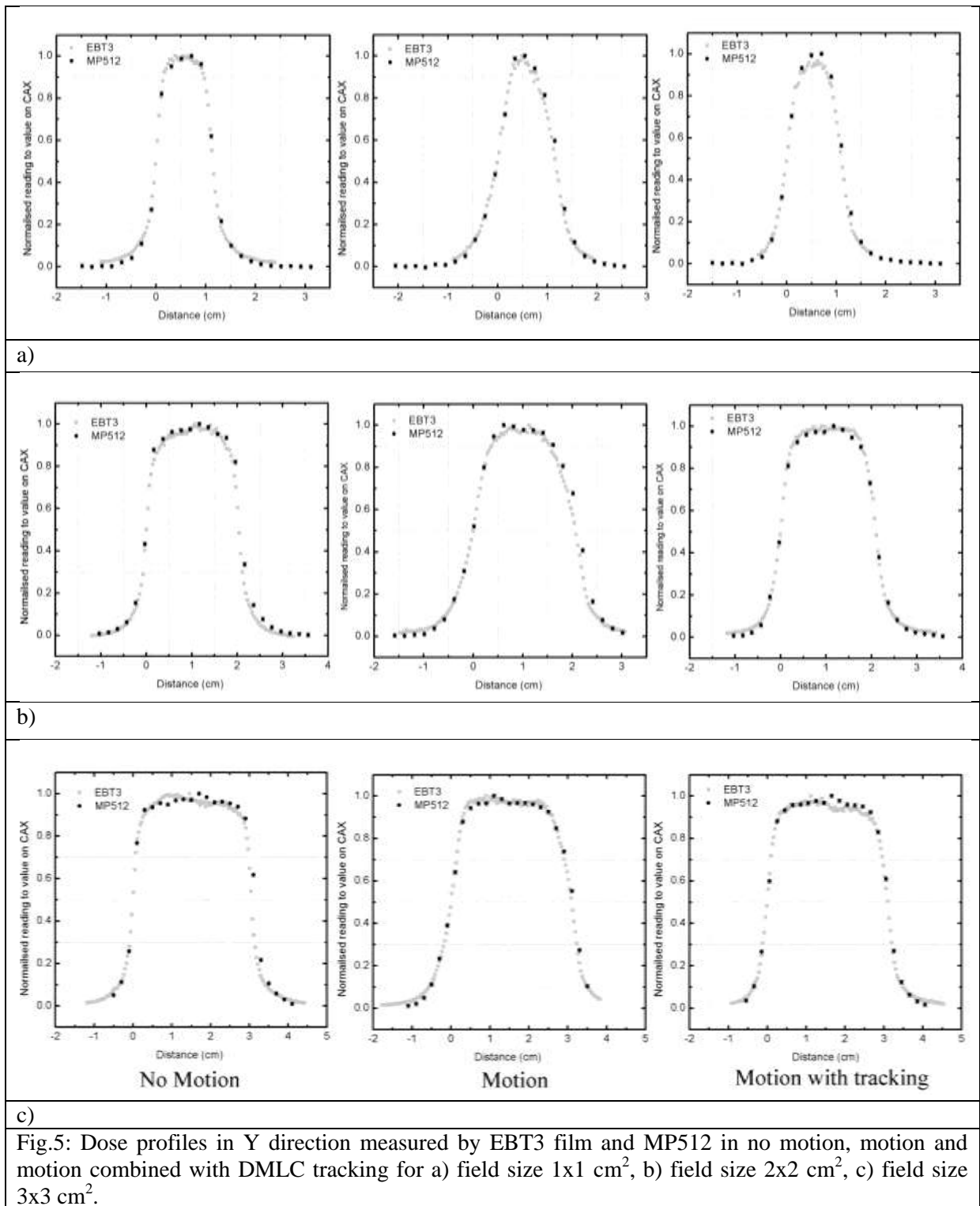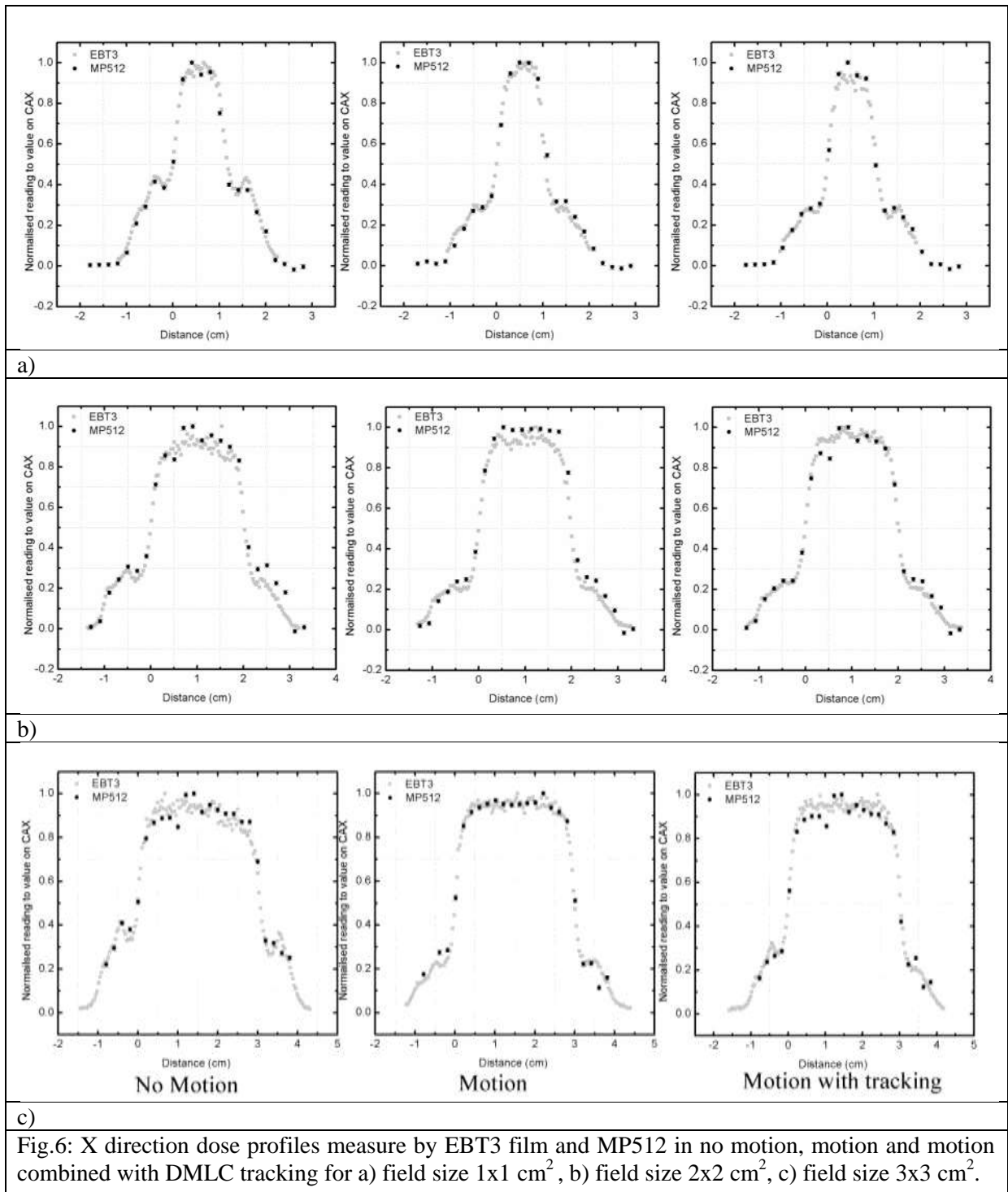
b. Beam profile measurements.

Fig.5 shows measurements of the beam profile along the Y direction for square radiation field sizes ranging from 1 to 3 cm. 2D responses for each radiation field measured by the MP512 was compared with 2D dose distributions measured by EBT3 films respectively. All MP512 profiles are normalised to the response of the central normal axis pixel (at row 11, column 12) while the profiles measured with EBT3 films are normalised to the average value of a 2x2 mm^2 area surrounding the central axis of the beam profile. Profiles measured by MP512 and EBT3 are aligned to the value of 50% of the response of the central pixel (11,12) and central axis dose value for MP512 and EBT3, respectively. Quantitative evaluation of the agreement between film and MP512 datasets has been performed by the means of MATLAB (Mathworks. Inc) generating a fit by the Curve Fitting Toolbox. The FWHM and the right hand side (RHS) penumbral width (80%-20%) are evaluated by interpolating the data points using the interpolation-shape-preserving fit and reported in Tab.2. The right hand side of the profile has been chosen because it is more representative to show the large distortion generated by the organ motion pattern adopted for this work. This effect is due to the offset of approximately 4 mm (Fig.2) generated by the motion towards the positive Y direction corresponding to the positive direction of the distance reported in Fig.5.

Tab.2: Summary of the comparison of FWHM and right hand side (RHS) penumbra of the Y direction square fields measured by MP512 and EBT3 film.

Modality	Square field size (cm)	EBT3		MP512	
		FWHM (cm)±0.01	RHS Penumbra (cm)±0.01	FWHM (cm)±0.01	RHS Penumbra (cm)±0.01
No-Motion	1	1.14	0.26	1.17	0.25
	2	2.04	0.27	2.10	0.30
	3	3.06	0.30	3.16	0.29
Motion	1	1.16	0.50	1.21	0.51
	2	2.07	0.54	2.15	0.56
	3	3.10	0.53	3.15	0.57
Motion+tracking	1	1.10	0.35	1.14	0.37
	2	2.10	0.34	2.10	0.38
	3	3.10	0.35	3.12	0.39

Fig.5: Dose profiles in Y direction measured by EBT3 film and MP512 in no motion, motion and motion combined with DMLC tracking for a) field size 1x1 cm^2, b) field size 2x2 cm^2, c) field size 3x3 cm^2.

Measurements confirm the impact of the tracking technique for mitigation of the dose smearing generated by the organ motion. The effectiveness can be quantitatively evaluated by considering the variation of the penumbra between no-motion and motion, with 2.4 mm average increase with uncorrected motion. When the tracking is activated, the variation is reduced down to 0.7 mm with an effective reduction of 70%. MP512 agrees with the measurements obtained by film within 3% and 0.4 mm for FWHM and penumbra width, respectively.

Fig.6: X direction dose profiles measure by EBT3 film and MP512 in no motion, motion and motion combined with DMLC tracking for a) field size 1x1 cm^2 , b) field size 2x2 cm^2, c) field size 3x3 cm^2.

345

Profiles measured by MP512 along the X direction are also presented in comparison with EBT3 film (Fig.6). The lung motion pattern adopted for this experiment presents an X lateral movement of approximately ±1 mm. This distance is not large enough to trigger the displacement of a leaf when the tracking system is activated because the minimum leaf width in X-direction is 2mm. Because tracking

350 is not so sensitive along the X direction in comparison to Y-direction, the shapes of the dose profiles obtained in case of the motion-tracking modality is more similar to the dose shape profiles obtained in

case of the motion modality rather than the one obtained in no-motion modality, for all the three field sizes. The pattern of the beam profiles below 30% of maximum dose is related to radiation leakage between tips of closed leaves and which are absent in the profiles measured in Y direction (Fig.5).

355   *c. Dynamic wedge measurement*

Fig.7 shows the dose deposition profiles of the no-motion, motion and motion with tracking of the dynamic wedge measured by MP512 considering a dose calibration factor of 5.81 nC/cGy. The difference between the no-motion and motion with tracking is that the integral response can reach a maximum difference of approximately +15% in the region corresponding to the right hand side
360   penumbra of the wedge while keeping the discrepancy with the no-motion scenario within -3% along the wedge. The comparison between no-motion and motion scenarios (with tracking not activated) shows an average difference of -18% along the wedge and a peak of +75% in the penumbra region with a displacement of approximately 8-10 mm of the dose distribution.
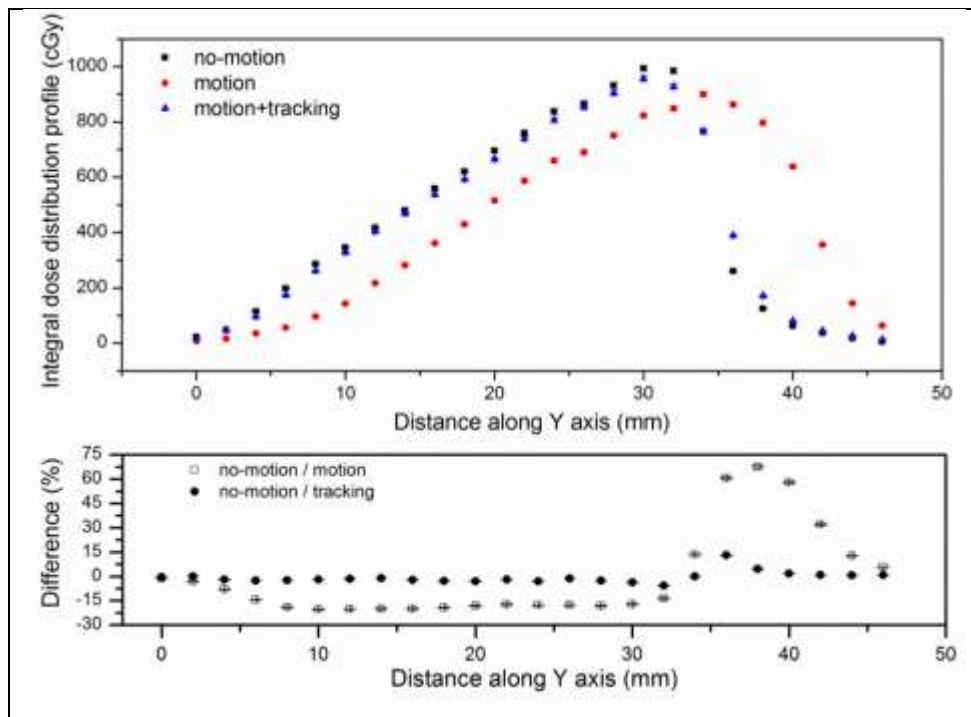

Fig.7: Dynamic wedge integral dose profiles along the central Y axis of the MP512 detector (upper panel); the percentage difference normalized to the no-motion peak integral dose response (lower panel).

365   Fig.8 shows the dynamic wedge measured by EBT3 film in the same experimental conditions used for MP512. The upper panel of the plot shows the value in absolute dose (cGy) after calibration and the lower panel the difference in percentage of the motion and tracking in comparison with the no-motion. The difference plot shows a very good agreement with the results obtained by MP512, with +70% of discrepancy for the penumbra region and -18% for the wedge region in the motion with no

370 tracking modality. Fig.9 shows the direct comparison of the wedge profiles measured by film and MP512.
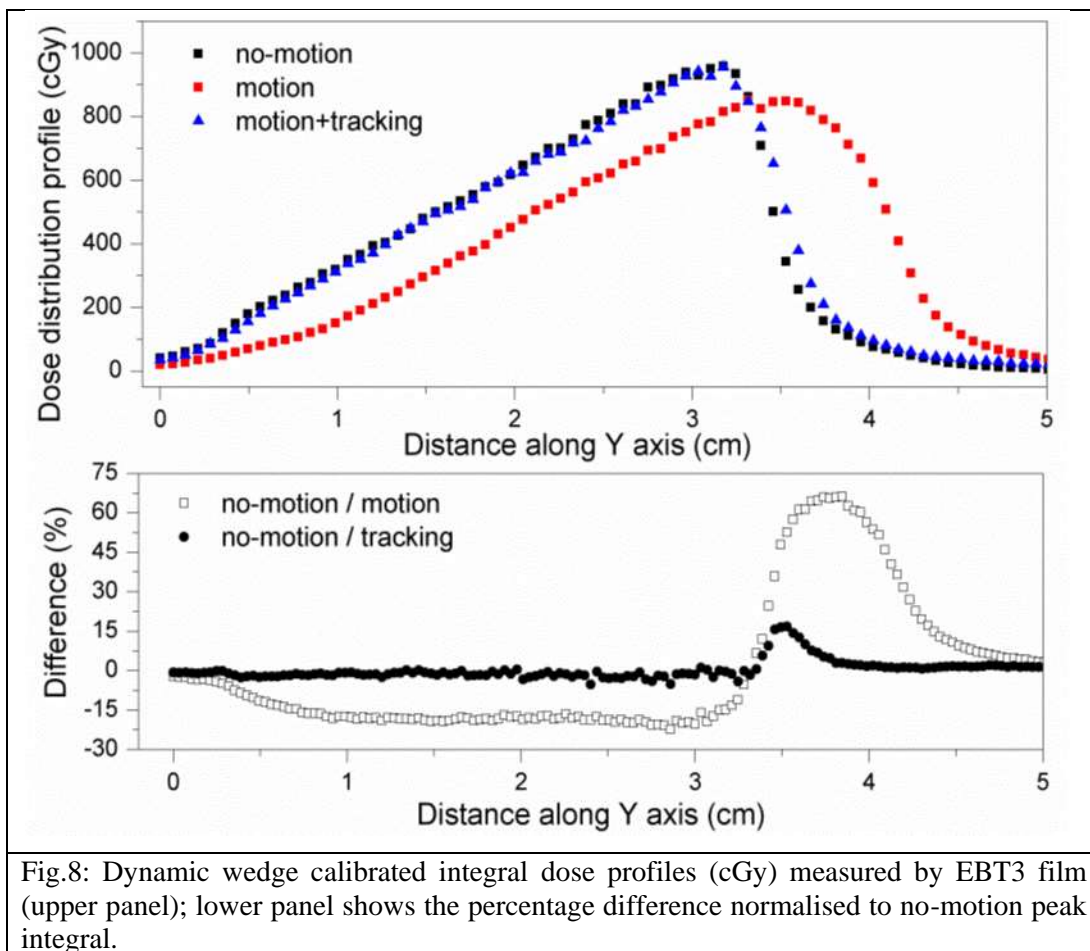

Fig.8: Dynamic wedge calibrated integral dose profiles (cGy) measured by EBT3 film (upper panel); lower panel shows the percentage difference normalised to no-motion peak integral.
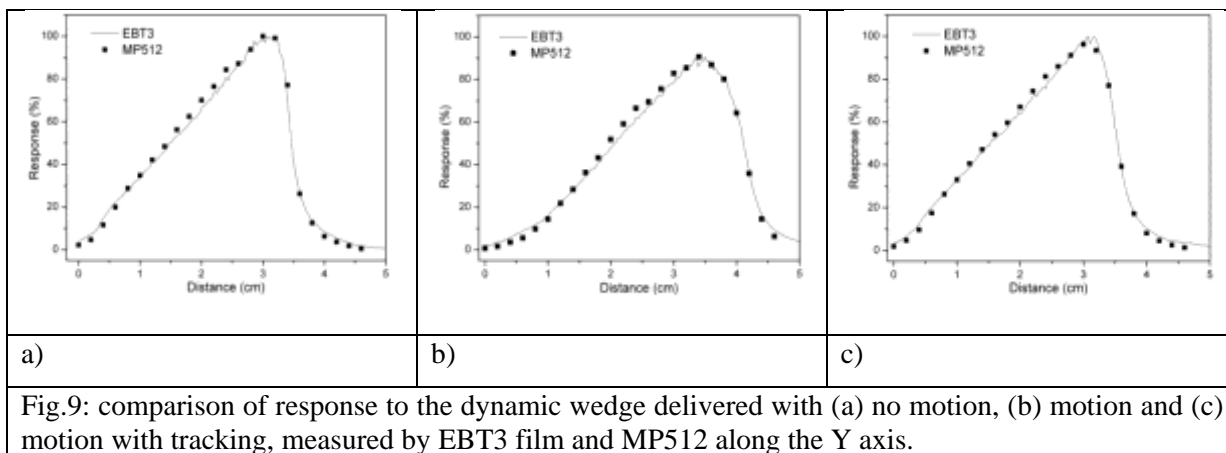

a)

b)

c)

Fig.9: comparison of response to the dynamic wedge delivered with (a) no motion, (b) motion and (c) motion with tracking, measured by EBT3 film and MP512 along the Y axis.

A detailed retrospective timing analysis of the single pixels' response as a function of time helps to
375 understand where the tracking system algorithm's performance are impaired and it is not able to reconstruct accurately the wedge profile. Fig.10 illustrates the charge accumulated per linac pulse as a

function of time recorded for the pixel receiving 50% of maximum charge among other pixels receiving dose during the dynamic wedge delivery in no-motion, motion and motion with tracking modality. These pixels correspond to pixel (11,13), pixel (8,13) and pixel (11,13) of the MP512 array, respectively. The chosen pixels are not the same because the dynamic wedge analysis aims to explore the timing distribution of the dose delivered, maintaining the dose constant (equivalent to the area of the dose as a function of time reported in Fig.10). The no-motion time trace is determined exclusively by the movement of the MLC providing the dynamic wedge. The slow change of response for the first 20 seconds is corresponding to exposure of the (11,13) pixel to the full unshielded radiation field by MLC. After approximately 20 seconds, charge decreasing corresponds to increasing of shielding by MLC motion and finally full shielding of the pixel. When the lung motion pattern is combined with the MLC movement a strong deviation of the time response of the pixel (8,13) in the motion mode from the time response of the pixel (11,13) in the case of no-motion mode is observed due to interplay effect. Observed spikes of over response and under response correspond to the maximum displacements of the pixel. Amplitude of these spikes increases when MLC edge is within the oscillation amplitude of the pixel due to the lung motion, leading to full shielding or full exposure of the pixel to the radiation field. The temporal pattern of these spikes during the interval 35-50 seconds is also affected by the convolution of the MLC movement and the relative pixel motion, as shown by the fast reducing amplitude of the signal from pixel (11,13) (in tracking mode). The DMLC tracking mitigates the displacement of the pixel in comparison with motion mode only during the first 20 seconds. However, even in this time interval, it is possible to observe small narrow negative spikes with increased amplitude in time. These short spikes match with the fastest motion components of the respiratory pattern of the lung. This effect leads to an average integral response for motion+tracking slightly smaller (approximately -3%) than in no-motion mode as presented in Fig.7 and Fig.8. When combination of wedge and lung motion reduces the variation speed of the dose rate in the pixel, DMLC compensation becomes effective again, reducing the discrepancy between no-motion and motion+tracking response. Considering the integral response of pixel (11,13), the interplay effect for motion+tracking mode is not essential as shown by the good agreement of the integral charge response in Fig.7 and Fig.8, because the most dose is delivered during the slow dose rate varying components, corresponding to the dose delivered when the position of the target maintains for a longer time the same position.
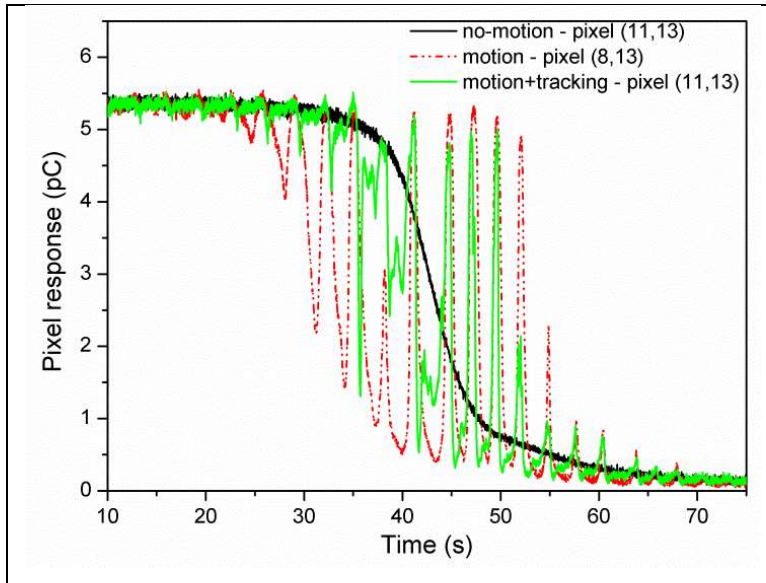
Fig.10: Charge deposition transient recorded by one MP512 pixel along the wedge profile which has accumulated 50% of the maximum integral charge deposited among all other pixels for three motion modalities.

The latency associated with the tracking algorithm, based on the error estimation and correction feedback has a measurable delay (approximately 230 ms [7]) between the acquisition of the beacons' positions provided by Calypso and the response of the MLC. A predictive algorithm could be used to improve the performance of the tracking system, as suggested by Srivastava et al. [26]. MP512 has the temporal and spatial resolution to be used to refine the parameters of the predictive algorithm by minimizing the pixel response oscillations generated by the fast transient components of the patient specific motion pattern adopted for the treatment verification.

Limitations

A limitation of this work is that it was a dosimetric study conducted using only one motion pattern and the movement is limited to the XY plane with no variation of the detector distance from the linac source. A variation in SSD contributes to a variation of the dose rate measured by the detector due to motion in Z-direction. This component could create uncertainties to estimate the performance of MP512 in determining the mitigation of the dose variation in X-Y direction by DMLC tracking system assuming that tumor is not deformable. A further study will investigate the effect of depth variation on the detector response in a full 4D motion patterns from different organs compared to film dosimeters. Another limitation of this study is the use of the gantry in a vertical fixed position instead of rotating around the phantom as in a real SBRT or SRS treatment scenario. MP512 angular response and the corresponding angular correction factors will be reported separately. Strategies to compensate the angular response of a monolithic silicon detector are well known and include applying either angular correction factors or placement of MP512 in a rotatable cylindrical phantom that rotates

synchronically with the gantry providing the beam incidence normally to the detector [27],[28]. Despite the more challenging design necessary for the phantom, this approach is feasible considering that HexaMotion is originally designed for Delta⁴ and is able to manage the weight associated with the cylindrical drum of the rotatable phantom.

Discussions and conclusions

The SBRT and SRS are radiation therapy technologies currently implemented widely on all types of linacs and allow conformal treatment even for small volume tumors. Organ motion during treatment is patient specific and can be taken into account in SBRT and SRS by increasing margins in PTV or using image guidance to adapt the radiation beam shape and intensity to the movable target. Such approach has been recently introduced clinically using the Calypso-guided MLC tracking system. In both cases, a high spatial and temporal resolution dose delivery QA system is required to provide real-time feedback to clinicians. Presently film only can provide direct dosimetry with adequate spatial resolution but still showing large limitations in terms of accuracy and real-time measurement.

CMRP has developed MP512, a high spatial and temporal resolution dosimetry system which, mimicking the moving tumor, measures 2D dose distributions and the effect of movement, simultaneously. MP512 consists of a 2D pixilated (512 pixels) monolithic thin silicon detector with a pixel size of 0.5x0.5 mm^2 and pitch of 2 mm. The sensor is readout by a fast front-end electronics which allows for pulse by pulse dosimetry and, in combination with a movable platform, reproduces patient specific tumor motion.

Use of MP512 in combination with the motion platform HexaMotion has been investigated by the use of a patient specific 3D (X, Y and time) lung motion pattern and by the electromagnetic motion tracking system Calypso. Verification of the motion compensation algorithm in controlling the DMLC effectively for accurate beam delivery to the movable target has been achieved, comparing the dose distribution measured by MP512 for static, movable and tracked beam delivery to the phantom.

The radiofrequency electromagnetic field emitted by Calypso induces fluctuations of the baseline current in electronic based dosimetry systems. Such issue has been overcome by the application of an aluminum shielding which encloses the detector maximizing the signal to noise ratio of the instrument. It was demonstrated that 2 mm thick aluminum shields effectively the electromagnetic radiation when it placed on the surface of a 10 mm thick solid water slab. Such configuration of the build-up material is equivalent to d_{max} for 6 MV photon beam and it has been proved by Monte Carlo simulations and by experimental measurements with an ionization chamber, that aluminum shield does not perturb the radiation field at depth higher than 14 mm for radiation field sizes of 1x1, 2x2 and 3x3 cm^2. PDDs with the shield for the aforementioned fields, are in agreement within 1% below d_{max} when compared to dose simulated in water without the aluminum shield. The design of the

electronic front end minimizes also the microphonic noise which shows no effect on the detector response when tested with the 3D lung motion pattern.

MP512 with designed build up is able to reconstruct the dose profiles in X and Y –directions for mentioned square radiation fields in case of no-motion, motion, and motion with tracking of the detector with a discrepancy within 0.4 mm and 4% in penumbra width and FWHM, respectively, when compared to EBT3 film.

MP512 is also able to record the instantaneous dose deposited pulse-by-pulse allowing for an accurate real time or retrospective analysis of the dose escalation measured by each pixel. Performance of motion adaption algorithm for DMLC in conjunction with Calypso motion tracking system was investigated by MP512 for typical lung motion pattern in case of a 3x3 cm^2 field size dynamic wedge delivered by the MLC. It was demonstrated that DMLC motion tracking in this case is excellent leading to dose discrepancy with stationary MP512 less than -3% along the wedge dose profile and a maximum discrepancy of +15% in penumbral region of the wedge. In case of absence of motion tracking an average dose difference of -18% along the wedge and a peak of +75% in the penumbra region were measured.

Retrospective analysis of temporal response of each pixel during the dynamic wedge delivery in case of motion tracking allowed investigating how DMLC and motion adaptive algorithm manage interplay effect due to MLC and target motion. It was demonstrated that existing algorithm is providing large instantaneous discrepancy in penumbral regions of the field where dose gradient is steep including movable penumbras determined by MLC motion. This effect is due to latency of the tracking algorithm as reported previously. This feature of the MP512 system is particularly useful when a motion predictive algorithm is adopted to drive the DMLC to tune the parameters of the tracking system maximizing its effectiveness.

References

1. Morales JE, Crowe SB, Hill R, Freeman N, Trapp JV "Dosimetry of cone-defined stereotactic radiosurgery fields with a commercial synthetic diamond detector" Med Phys. 41(11):111702, 2014, doi: 10.1118/1.4895827P.

2. Keall et al. "Electromagneticiguided dynamic multileaf collimator tracking enables motion management for intensity-modulated arc therapy" Int. J. Radiation Oncology Biol. Phys., Vol. 79, No. 1, pp. 312–320, 2011

3. Menten, M. J., Guckenberger, M., Herrmann, C., Krauß, A., Nill, S., Oelfke, U., & Wilbert, J. (2012). Comparison of a multileaf collimator tracking system and a robotic treatment couch tracking system for organ motion compensation during radiotherapy. Medical Physics, 39(11), pp.7032–41. doi:10.1118/1.4761868

4. Lang S, Zeimetz J, Ochsner G, Schmid Daners M, Riesterer O, Klöck S. "Development and evaluation of a prototype tracking system using the treatment couch" Med Phys. 41(2):021720. doi: 10.1118/1.4862077, 2014

5. Falk, M., Munck, P., Keall, P., Cattell, H., Chul, B., Poulsen, P., et al. (2010). Real-time dynamic MLC tracking for inversely optimized arc radiotherapy. Radiotherapy and Oncology, 94(2), 218–223. doi:10.1016/j.radonc.2009.12.022

6. J. Wong, N. Wright, S. Dimmer, B. Friemal, J. Newell, A. Silber, T. Mate, J. Pouilot "Patient Positioning and Setup - Beacon" http://radonc.ucsf.edu/research_group/jpouliot/tutorial/hu/Lesson20.htm (access 06/01/2015)

7. P.J. Keall, E. Colvill, R. O'Brien, J.A. Ng, Per Rugaard Poulsen, Thomas Eade, Andrew Kneebone, J.T. Booth "The first clinical implementation of electromagnetic transponder-guided MLC tracking" Med. Phys. 41 (2), 020702-1, 2014

8. Smith, R. L., Sawant, A., Santanam, L., Venkat, R. B., Newell, L. J., Cho, B. Chul, (…) Parikh, P. J. (2009). Integration of Real-Time Internal Electromagnetic Position Monitoring Coupled With Dynamic Multileaf Collimator Tracking: An Intensity-Modulated Radiation Therapy Feasibility Study. International Journal of Radiation Oncology Biology Physics, 74, 868–875. doi:10.1016/j.ijrobp.2009.01.031

9. Sawant, A., Smith, R. L., Venkat, R. B., Santanam, L., Cho, B., Poulsen, P. et al. (2008). Toward Submillimeter Accuracy in the Management of Intrafraction Motion: The Integration of Real-Time Internal Position Monitoring and Multileaf Collimator Target Tracking. International Journal of Radiation Oncology Biology Physics, 74, 575–582. doi:10.1016/j.ijrobp.2008.12.057

10. Indra, J. Das, Ding George X., Ahnesjö Anders "Small fields: Nonequilibrium radiation dosimetry" Medical Physics, 2008. 35(1): p. 206-215.

11. Wagner A1, Crop F, Lacornerie T, Vandevelde F, Reynaert N. "Use of a liquid ionization chamber for stereotactic radiotherapy dosimetry" Phys. Med. Biol. 58(8), pp:2445-59 (2013) doi: 10.1088/0031-9155/58/8/2445

12. Lacroix, F., Archambault, L., Gingras, L., Guillot, M., Beddar, a. S., & Beaulieu, L. (2008). Clinical prototype of a plastic water-equivalent scintillating fiber dosimeter array for QA applications. Medical Physics, 35(8), 3682. doi:10.1118/1.2953564

13. Fontbonne, J. M., Iltis, G., Ban, G., Battala, A., Vernhes, J. C., Tillier, J., … Motin, J. C. (2002). Scintillating fiber dosimeter for radiation therapy accelerator. IEEE Transactions on Nuclear Science, 49 I, 2223–2227. doi:10.1109/TNS.2002.803680

14. Beddar, A.S., et al., A miniature "scintillator-fiberoptic-PMT" detector system for the dosimetry of small fields in stereotactic radiosurgery. IEEE Transactions on Nuclear Science, 2001. 48(3): p. 924-928.

15. A.H. Aldosari, M. Petasecca, A. Espinoza, M. Newall, I. Fuduli, C. Porumb, S. Alshaikh, Z.A. Alrowaili, M. Weaver, P. Metcalfe, M. Carolan, M.L.F. Lerch, V. Perevertaylo, A.B. Rosenfeld "A 2D silicon detectors array for QA in Stereotactic Radiotherapy: MagicPlate-512" – Medical physics 2014; 41(9):091707

16. Texas Instruments, 64 Channel Analog Front End for Digital X-Ray Detector. September 2009; Datasheet available from: http://www.ti.com/lit/ds/slas672/slas672.pdf

17. Fuduli, M.K. Newall, A.A. Espinoza, C.S. Porumb, M.Carolan, M.L.F. Lerch,P. Metcalfe, A.B. Rosenfeld, M. Petasecca "Multichannel Data Acquisition System comparison for Quality Assurance in external beam radiation therapy" – Radiation Measurements (accepted on 12 May 2014) doi: 10.1016/j.radmeas.2014.05.016.

18. Yamazaki, S Nakane, H.; Tanaka, A., IEEE Transactions on Instrumentation and Measurement, Vol.51,Iss.4, 2002, pp: 810- 814

19. Kai Huang, William S. Bice, Jr., and Oscar Hidalgo-Salvatierra "Characterization of an in vivo diode dosimetry system for clinical use" JOURNAL OF APPLIED CLINICAL MEDICAL PHYSICS, VOLUME 4, NUMBER 2, SPRING 2003

20. Agostinelli et al. "Geant4-a simulation toolkit" Nucl. Instrum. Methods Phys. Res. A, 506, 2003, pp. 250-303

21. BM Oborn and M Williams and M Bailey and M G Carolan "IMRT treatment Monitor Unit verification using absolute calibrated BEAMnrc and Geant4 Monte Carlo simulations" Journal of Physics: Conference Series, 489 (1), 2014, 012020

22. Wong, J.H.D. et al. "Characterization of a novel two dimensional diode array the magic plate as a radiation detector for radiation therapy treatment" Medical Physics 39 (5), pp. 2544-2558, 2012

23. Westermark, M., et al., Comparative dosimetry in narrow high-energy photon beams. Physics in Medicine and Biology, 2000. 45(3): p. 685-702

24. Butson, M.J., T. Cheung, and P.K.N. Yu, Scanning orientation effects on Gafchromic EBT film dosimetry. Australasian Physics & Engineering Sciences in Medicine, 2006. 29(3): p. 281-284.

25. Andrés, C., et al., A comprehensive study of the Gafchromic EBT2 radiochromic film. A comparison with EBT. Medical physics, 2010. 37(12): pp. 6271-6278.

26. Srivastava V, Keall P, Sawant A, et al. "Accurate prediction of intra-fraction motion using a modified linear adaptive filter" Med Phys 2007;34:2546

27. PA Jursinic, Sharma R, Reuter J "MapCHECK used for rotational IMRT measurements: step-and-shoot, TomoTherapy, RapidArc" Med. Phys. 37(6), pp.2837-46, 2010

28. Van Esch A, Clermont C, Devillers M, Iori M, Huyskens DP "On-line quality assurance of rotational radiotherapy treatment delivery by means of a 2D ion chamber array and the Octavius phantom" Med. Phys. 34(10), pp.3825-37, 2007